Preparation and Characterization of a Truncated Form of Phthalate Dioxygenase Reductase That Lacks an Iron−Sulfur Domain†

George T. Gassner and David P. Ballou*

Department of Biological Chemistry, University of Michigan, Ann Arbor, Michigan 48109-0606

Received April 14, 1995; Revised Manuscript Received July 19, 1995®

ABSTRACT: Phthalate dioxygenase reductase (PDR) is the electron transferase component of the phthalate dioxygenase system. It is a modular enzyme consisting of distinct iron−sulfur, flavin mononucleotide (FMN) and pyridine nucleotide binding domains. We have taken advantage of this modularity and removed the 10-kDa iron−sulfur domain by selective proteolytic cleavage between residues N229 and T230 in a solvent-accessible peptide that links the iron-sulfur and pyridine nucleotide binding domains. The resulting PDR(−FeS) has a molecular weight of 25 792 ± 10 and the same amino terminus as the native PDR. It has spectral features that are very similar to the flavin component of the PDR absorbance spectrum. Remarkably, despite the magnitude of this structural modification, the kinetic, redox, and pyridine nucleotide binding properties of PDR(−FeS) are very similar to those reported for PDR [Gassner, G., *et al.* (1994) *Biochemistry 33*, 12184−12193]. The principal mechanistic feature distinguishing PDR(−FeS) from PDR is the inability of the attenuated enzyme to carry out intramolecular electron transfer. The reaction of PDR(−FeS) with NADH consists of binding and the formation of an initial Michaelis complex (MC-1′) ($K_d \sim 25$ μM), isomerization of the enzyme (120 s^{-1}) to form a charge-transfer complex with FMN (CT-1′), hydride transfer to the FMN (76 s^{-1}) with formation of a second charge-transfer complex (CT*′), and finally release of nicotinamide adenine dinucleotide (NAD) (58 s^{-1}) from the reduced enzyme. The rate of NAD release from PDR(−FeS) is nearly the same as the rate of NAD release and intramolecular electron transfer in the reductive half-reaction of PDR, which supports the idea that the release of NAD triggers intramolecular electron transfer in PDR. The midpoint potential of the oxidized/semiquinone couple of PDR(−FeS) (−170 mV) is the same as the value measured for PDR. A value of −235 mV is measured for the midpoint potential of the semiquinone/hydroquinone couple of PDR(−FeS), which is ~50 mV more positive than the PDR_{2e^-}/PDR_{3e^-} redox couple at pH 7. NAD binds to PDR(−FeS) about 20-fold more weakly than does NADH; the enzyme redox state has no significant influence on pyridine nucleotide binding affinity.

The phthalate dioxygenase system (PDS)[1] isolated from *pseudomonas cepacia* consists of two protein components: (a) phthalate dioxygenase (PDO), a multimer of identical subunits, each containing one [2Fe−2S] Rieske center and one mononuclear hexacoordinate ferrous iron site, and (b) phthalate dioxygenase reductase (PDR), a monomeric FMN and plant-type ferredoxin-containing protein (Batie *et al.*, 1986). PDR functions in the transmission of electrons from reduced pyridine nucleotide (NADH) to the Rieske center of PDO. Ultimately these electrons are used in the activation of molecular oxygen bound at the mononuclear site of PDO during the dihydroxylation of phthalate (Ballou & Batie, 1988).

Resolution of the oxygenase and reductase components on separate peptide components is a common theme among the bacterial dioxygenases (Batie *et al.*, 1992). Similar multicomponent peptide arrangements also exist for other bacterial systems involved in the NADH-dependent monooxygenation of electronically stabilized carbon compounds such as toluene (Yeh *et al.*, 1977), benzoate (Yamaguchi & Fujisawa, 1982), methane (Lund *et al.*, 1985), and cresol (Hopper, 1976). Although these systems are quite complex when considered in concert, their modular peptide structure in many cases allows for the independent study of reductase, intermediate electron transferase, and hydroxylase components. Thus, the NADH-dependent oxygenases of bacteria provide a simplified model for the kinetics of complex electron transfer reactions, such as those occurring in photosynthetic (Boxer, 1990) and respiratory (Wikström *et al.*, 1981) electron transfer chains.

We have taken a stepwise approach to studying the electron transfer reactions in the phthalate system by first investigating the anaerobic reactions of PDR with pyridine nucleotides in the absence of PDO. Exclusion of PDO from the reduction reaction facilitates the interpretation of kinetic data by significantly decreasing the mechanistic and spectral

† Supported by U.S. Public Health Service Grant GM 20877.

* To whom correspondence should be addressed at the Department of Biological Chemistry, University of Michigan, Medical Science Building I, Box 0606, Ann Arbor, MI 48109-0606.

® Abstract published in *Advance ACS Abstracts,* October 1, 1995.

[1] Abbreviations: Fl_{ox}, oxidized flavin; Fl_{sq}, semiquinone flavin; Fl_{hq}, hydroquinone flavin; PDS, phthalate dioxygenase system; PDR, phthalate dioxygenase reductase, HQ, hydroquinone flavin (oxidized iron−sulfur state of phthalate dioxygenase reductase); SQ, semiquinone flavin (reduced iron−sulfur state of phthalate dioxygenase reductase); PDO, phthalate dioxygenase; (−FeS), the iron−sulfur domain has been removed by proteolytic cleavage; (apoFeS), the iron−sulfur center has been disassembled with mersalyl acid; (+FeS), the iron−sulfur center has been reconstituted with iron and inorganic sulfide; (apoFMN), the flavin mononucleotide has been removed by dialysis against urea; NAD (NADH), nicotinamide adenine dinucleotide (reduced form); LC-MS, liquid chromatography−mass spectroscopy; PCA, protocatechuate; PCD, protocatechuate dioxygenase; PMSF, phenylmethanesulfonyl fluoride; DCPIP, dichlorophenolindophenol.

0006-2960/95/0434-13460$09.00/0

complexity of the reduction reaction. These studies have allowed us to identify steps of pyridine nucleotide binding, hydride transfer (from NADH to oxidized FMN), intramolecular single electron transfer (from FMN to the [2Fe−2S] center), and release of oxidized pyridine nucleotide in the reductive half-reaction of PDR (Gassner *et al.*, 1994).

The crystal structure of PDR reveals a highly modularized iron-sulfur flavoprotein consisting of distinct N-terminal FMN binding, central pyridine nucleotide binding, and C-terminal [2Fe−2S] domains. It also shows that the 8-methyl group of the FMN bound to PDR is only 4.7 Å from the [2Fe−2S] center (Correll *et al.*, 1992). Based on studies of solvent accessibility (Massey & Hemmerich, 1980; Ghisla & Massey, 1986) and rapid kinetic studies of intermolecular electron transfer between reduced flavodoxin and electron acceptors (Jung & Tollin, 1981), precedent exists for the 8-methyl group of protein-bound flavin to function as a conduit for electron transfer. Correlations have been made in accordance with Marcus theory (Marcus & Sutin, 1985) that relate experimental measurements of thermodynamic driving force, distance separating the donor and acceptor, and magnitude of the rate constant for electron transfer. On this basis, electron transfer in PDR is predicted to be quite rapid. Surprisingly, our kinetic studies on native PDR (Gassner *et al.*, 1994) indicate an observed rate of intramolecular electron transfer of only 35 s^{-1}.

Since the intramolecular electron transfer and NAD release steps are kinetically indistinguishable, we have proposed that NAD bound to PDR in the Fl_{red}-to-NAD charge-transfer complex, which is generated immediately following hydride transfer from NADH to the FMN moiety, may block electron transfer by either: (A) transiently raising the flavin redox potential to a value that thermodynamically disfavors the electron transfer event or (B) effecting a structural change that disrupts the pathway of electron transfer.

Comparison of the crystal structures of PDR and ferredoxin−NADP reductase (FNR) indicates significant similarities (Correll *et al.*, 1993). The structure of FNR closely overlaps the peptide backbone of the pyridine nucleotide- and FMN-binding domains of PDR. These enzymes are apparently close evolutionary relatives; however, the ferredoxin component of the FNR system is a separate water-soluble peptide rather than a covalently attached domain structure. The similarity of PDR to the ferredoxin/ferredoxin−NADP reductase complex and to the type II bacterial dioxygenases, in which flavin- and ferredoxin-binding domains reside on separate peptides (Batie *et al.*, 1992), suggested that domain components of PDR might be stable in solution as separate peptide units. In this paper we describe the properties of PDR(−FeS), a stable truncated form of PDR that lacks an iron−sulfur domain. This form of PDR is incapable of intramolecular electron transfer but retains all of the behavior of native PDR in its reactions with pyridine nucleotides. The properties of PDR(−FeS) emphasize the modular nature of PDR and reinforce the notion that PDR is a good model for electron transferases that employ flavins and [2Fe−2S] centers.

MATERIALS AND METHODS

Disassembly and Reassembly of the [2Fe−2S] and FMN Centers of PDR. Standard approaches to flavin removal (Husain & Massey, 1978) were screened. The only technique found to selectively remove the FMN from PDR was dialysis against 4 M urea at ice temperature. Following dialysis, the sample was gel-filtered over a Bio-Rad G-10 desalting column. Light brown fractions were collected with the spectral characteristics of plant-type ferredoxin.

Procedures similar to those used in the disassembly and reconstitution of ferredoxins (Malkin & Rabinowitz, 1966) were applied to PDR. The [2Fe−2S] center of PDR was disassembled by titration with mersalyl (Aldrich Chemical Co.), prepared as an 8.5 mM stock in 100 mM pH 8 HEPES buffer. A 10−20-fold molar excess of mersalyl was sufficient for complete disassembly of the iron center. Following titration, the PDR(apoFeS) sample was gel-filtered through a Bio-Rad G-10 column to remove excess mersalyl and then concentrated in an Amicon Centricon-30 centrifugal concentrator. Each of these procedures results in a fractional loss of FMN from the protein. The remaining FMN was effectively removed from PDR(apoFeS) after 3−4 cycles of gel filtration and Centricon-30 concentration, resulting in PDR(apoFeS,apoFMN).

The [2Fe−2S] centers of PDR(apoFeS) and PDR(apoFeS,-apoFMN) were successfully reconstituted after incubation of these samples (on the order of 1 mg per milliliter) at 4 °C for 10 min in 75 mM HEPES buffer (pH 8) containing 50 mM β-mercaptoethanol, 1 mM ferrous ammonium sulfate, and 1 mM sodium sulfide. A green polymeric side product was pelleted by centrifugation at 5000 rpm for 5 min. The resulting dark brown supernate was concentrated by ultrafiltration. The protein component of this mixture was recovered after removal of soluble inorganic iron sulfide by G-10 gel filtration. PDR(apoFeS) reconstituted with a [2Fe−2S] center is referred to as PDR(+FeS). PDR(apoFeS,-apoFMN) that has been reconstituted with a [2Fe−2S] center is referred to as PDR(+FeS,apoFMN).

Preparation of PDR(−FeS). Bovine pancreas α_4-chymotrypsin (Boehringer Mannheim Biochemicals) (200 μL of a 2 mg·mL^{-1} stock solution was added to 4 mL of 90 μM PDR in 100 mM HEPES buffer, pH 8, containing 95 μM $CaCl_2$. The digestion mixture was incubated at 25 °C in a large quartz cuvette. Spectra were recorded periodically, and the extent of the reaction was assessed by monitoring the absorbance ratio, A_{462}/A_{538}. This ratio increased from an initial value of 3 to a final value of 7 over the course of a 250-min reaction, consistent with a selective proteolysis of the [2Fe−2S] domain. The reaction was terminated by addition of 20 μL of 11.5 mM PMSF (Sigma Chemical Co.). The mixture was incubated at 4 °C for 24 h and then brought to 5 mM in EDTA to remove free iron and calcium from solution. The sample was then passed over a Bio-Rad G-10 desalting column equilibrated in 100 mM HEPES buffer, pH 8, and finally concentrated by Centricon-30 ultrafiltration (Amicon). In addition to concentrating the sample, the ultrafiltration step presumably removes low molecular weight proteolytic fragments of the [2Fe−2S] domain. On the basis of the absorbance spectrum and the results of SDS−PAGE, the sample is about 95% converted to PDR(−FeS) at this stage. The final PDR(−FeS) preparation had an A_{462}/A_{538} ratio of ~11. PDR(−FeS) prepared in this fashion can be stored in 80 mM HEPES buffer, pH 8, containing 20% glycerol (v/v) at 4 °C for at least 1 month with no detectable degradation.

SDS−PAGE, N-Terminal Sequence Analysis, and Electrospray Mass Spectrometry. Samples were collected peri-

odically during the digestion of PDR with chymotrypsin and then denatured in buffer containing 5 mM PMSF. These samples were applied to a 10% Laemmli-type polyacrylamide gel and resolved electrophoretically using a Hoefer minigel apparatus run at a constant current of 20 mA. The molecular weight of PDR(−FeS) was estimated by interpolation of a plot of R_f values of protein standards vs molecular weight. Based on the relative intensities of bands representative of PDR and PDR(−FeS), it is estimated that the PDR(−FeS) preparation is contaminated by no more than ~5% PDR. A sample of the 250-min digest was submitted to the University of Michigan Protein Core. The N-terminal amino acid sequence was determined from the results of 7 cycles of Edman degradation using an Applied Biosystems Model 473 sequenator. Residues 3−7 of the PDR(−FeS) sequence are an exact match for the N-terminal residues (3−7) of native PDR. The identity of the first two N-terminal amino terminal residues could not be determined with certainty. The molecular weight of PDR(−FeS) was determined by LC-MS: Sample was applied to a 1-mm × 8-mm C-8 column and eluted at 20 μL·min^{-1} with a gradient of acetonitrile (4−60%) containing 0.1% TFA. Electrospray mass spectra were acquired with a Fisons/VG platform single-quadrupole mass spectrometer.

Titrations and Oxidation−Reduction Potential Determinations. Anaerobic titrations and reductions were carried out in a specially designed anaerobic quartz cuvette [similar to the type described by Burleigh *et al.* (1969)]. Anaerobic solutions were prepared by exchanging the aerobic atmosphere above the solution with argon containing less than 0.5 ppm oxygen. All solutions used in anaerobic reactions included 100 μM PCA and 1 μM PCD as an oxygen-scavenging system (Bull & Ballou, 1981). Photochemical reductions (Massey & Hemmerich, 1977, 1978) were performed in a thermostated bath maintained at 4 °C. Midpoint potentials were determined using the xanthine oxidase system as a source of reducing equivalents (Massey, 1991) and employing the indicator dyes listed below to monitor the redox state of the solution as the reduction proceeded. NAD (98%) and NADH (100%) used in reductive titrations, determinations of K_d, and the kinetic studies described below were purchased from Boehringer Mannheim Biochemicals. Potassium ferricyanide used in oxidative titrations was purchased from Mallinckrodt Biochemicals. Xanthine, xanthine oxidase, 5-deazaflavin, and 1-OH-phenazine used in redox titrations were gifts from Dr. V. Massey. The redox indicators, anthraquinone-1,5-disulfonic acid, anthraquinone-2-sulfonic acid, methyl viologen, and benzyl viologen were from the Aldrich Chemical Co. Spectra were recorded using a Perkin-Elmer Lambda-6 split-beam spectrophotometer.

Stopped-Flow Kinetic Studies. Stopped-flow studies were performed with a Hi-Tech SF-61 stopped-flow spectrophotometer. This instrument has a 2-ms dead time and requires only 35−40 μL of sample per shot. This instrument was set up for facile interconversion between single-wavelength photomultiplier (PMT) mode and diode array mode, making both forms of data collection accessible in a single experiment. Single-wavelength data were collected logarithmically with respect to time using a MacADIOS interface board equipped with a 16-bit analog-to-digital converter. This was controlled by KISS software and hardware from Kinetic Instruments, Inc. installed in a Macintosh IIcx. Diode array data were collected using Hi-Tech hardware and software installed in a 66-MHz DX2 Gateway computer. NADD used in deuterium isotope effect studies was generated enzymatically from NAD as described previously (Gassner *et al.*, 1994).

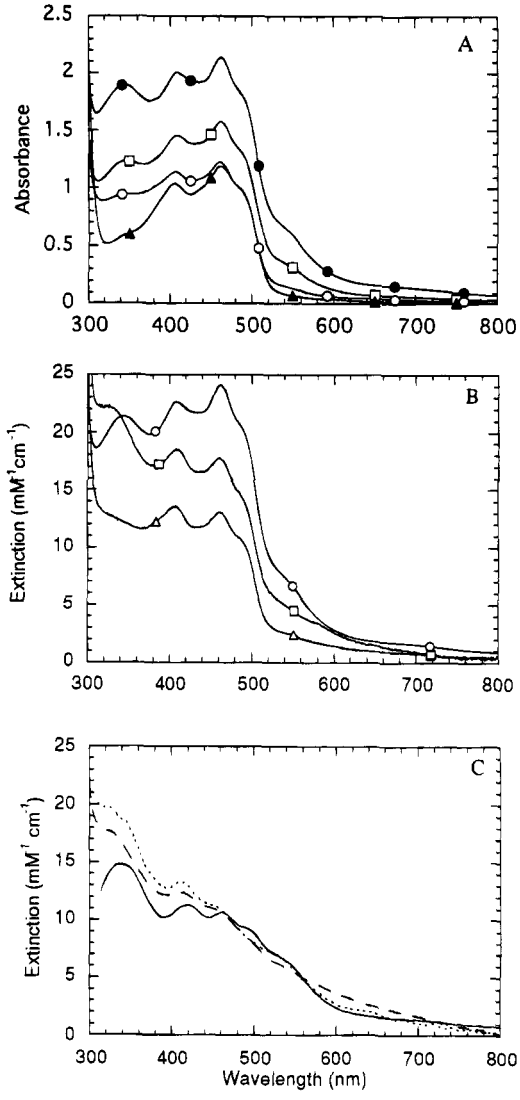

FIGURE 1: (A) Treatment of PDR with chymotrypsin: (●) spectrum of oxidized PDR (3.2 mg·mL^{-1}) in 100 mM HEPES buffer, pH 8, containing 100 μM $CaCl_2$ at 25 °C; spectra recorded (□) 60 min and (○) 255 min after addition of the α_4-chymotrypsin (final concentration 100 μg·mL^{-1}); (▲) spectrum taken after addition of 55 μM PMSF, incubation in 5 mM EDTA for 24 h, and gel filtration. (B) Comparison of spectra: (○) PDR, (□) PDR(+FeS), and (△) PDR (apoFeS). (C) (···) PDR(apoFMN) spectrum, (- - -) PDR(−FMN) spectrum, and (—) the difference between the initial and final spectra (● − ▲) presented in panel A.

RESULTS

Characterization of PDR(−FeS). Digestion of PDR using α_4-chymotrypsin was found to result in a selective proteolysis of the [2Fe−2S] domain that is accompanied by changes in the visible absorbance spectrum consistent with the destruction of the [2Fe−2S] center (Figure 1A). Similar spectral changes occur when the [2Fe−2S] center of PDR is disassembled by titration with mersalyl acid (Figure 1B). Subtraction of the normalized, final absorbance spectrum from the PDR starting spectrum gives an approximate spectrum of the [2Fe−2S] domain of PDR, which is quite similar to the spectrum of adrenodoxin (Figure 1C) (Gassner

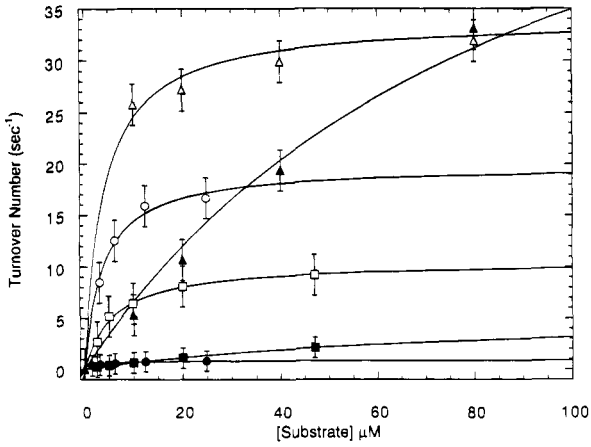

FIGURE 2: Saturation kinetics of the reaction of PDR and PDR(−FeS) with various electron acceptors. Reactions were performed anaerobically in pH 8 HEPES containing saturating NADH (435 μM) at 4 °C: Reaction of 1 μM PDR(−FeS) (solid symbols) or PDR (open symbols) with (●, ○) cytochrome *c*, (■, □) DCPIP, and (▲, △) $K_3Fe(CN)_6$.

et al., 1994). An extinction coefficient at 462 nm of 13.4 $mM^{-1}\cdot cm^{-1}$ was estimated for oxidized PDR(−FeS) on the basis of titration with NADH (data not shown).

Residues 3−7 of the N-terminal sequence of PDR(−FeS) (P-Q-E-D-G) were shown by amino acid sequencing to match the N-terminal sequence of PDR (Correll *et al.*, 1992). The molecular weight of PDR(−FeS) was determined by electrospray mass spectrometry to be 25 792 ± 10 Da. From the protein sequence deduced from the DNA sequence (Gerbin Zylstra, personal communication), the dominant chymotrypsin cleavage site is located in the sequence T-N-T, with the actual cleavage occurring between residues N-229 and T-230. This sequence falls in a solvent-exposed linker region of the protein (Correll *et al.*, 1992). Chymotrypsin cleaves peptides most frequently at the C-side of aromatic amino acid residues and with lower frequency after leucine, methionine, asparagine, and glutamine residues (Neil *et al.*, 1966). Other more favorable cleavage sequences scattered throughout the PDR molecule are apparently not attacked due to their inaccessibility. After cleavage from the main chain, the [2Fe−2S] domain is selectively destroyed. During the proteolytic digestion, multiple chymotryptic cleavage sites in the [2Fe−2S] domain may become accessible after the initial release of this domain from the rest of the protein. We were not able to detect the [2Fe−2S] domain fragment in SDS gels.

The steady-state kinetics of electron transfer from PDR and PDR(−FeS) to cytochrome *c*, DCPIP, and $K_3Fe(CN)_6$ are compared in Figure 2. A hyperbolic dependence of the reaction rate as a function of acceptor concentration was observed in all cases. The K_m of cytochrome *c* (3.3 ± 0.7 μM) is the same with either PDR or PDR(−FeS) as the electron donor. However, V_{max} values of the reactions with cytochrome *c* as the electron acceptor differ significantly. In the reaction of PDR with cytochrome *c*, V_{max} = 19.8 ± 0.9 s^{-1}, whereas V_{max} = 0.89 ± 0.03 s^{-1} for PDR(−FeS). It can be concluded that the iron−sulfur domain must play a significant role in the transmission of electrons from PDR to cytochrome *c*. It is likely that the cytochrome *c* reductase activity associated with the PDR(−FeS) preparation is due

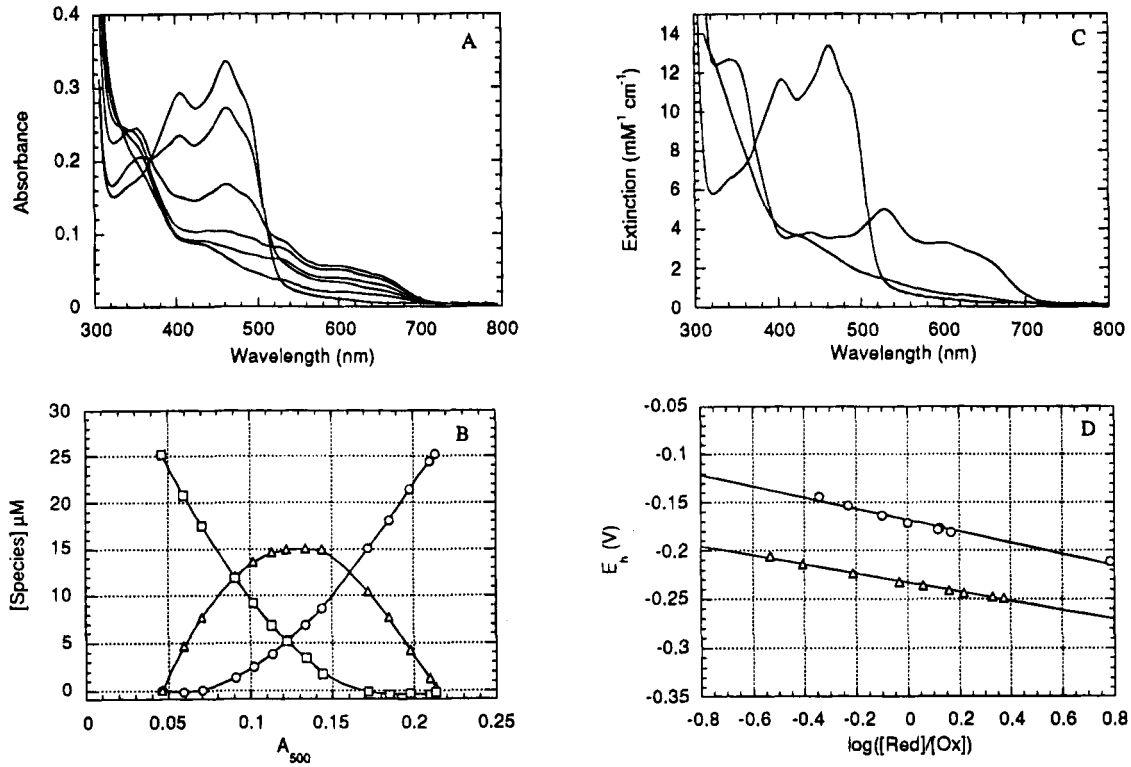

FIGURE 3: (A) Xanthine oxidase-mediated reduction of PDR(−FeS). The upper trace (at 460 nm) is the spectrum of 25.3 μM oxidized PDR(−FeS) in 20 mM potassium phosphate buffer, pH 7.0, at 30 °C. The lower five traces are selected spectra taken at various times during the reduction of PDR(−FeS) using the xanthine oxidase system (12.8 nM xanthine oxidase, 33 μM xanthine, and 20 μM benzyl viologen). (B) Calculated species concentrations (see eqs 1−3 in the text) plotted as a function of the extent of the xanthine oxidase-catalyzed reduction reaction: (□) oxidized, (△) semiquinone, and (○) fully reduced PDR(−FeS). (C) Pure oxidized, semiquinone, and fully reduced PDR(−FeS) spectra (upper, middle, and lower traces at 500 nm). (D) Log plot for the determination of PDR(−FeS) semiquinone (○) and hydroquinone (△) potentials (see text for details).

to contamination with PDR (~5% detected by SDS−PAGE).

The K_m of DCPIP in the reaction PDR(−FeS) is about 10-fold greater than in the reaction with PDR (74 ± 12 μM vs 6.0 ± 0.7 μM). V_{max} values for the reactions of PDR and PDR(−FeS) with DCPIP are 10.5 ± 0.4 s^{-1} and 5.5 ± 0.6 s^{-1}, respectively. Thus, it appears that the flavin of PDR(−FeS) is able to transfer electrons to DCPIP directly. However, the iron−sulfur domain of PDR greatly increases the catalytic efficiency (V_{max}/K_m) of PDR relative to PDR(−FeS) in the reduction of DCPIP.

Values of both V_{max} and K_m are larger in the reaction of PDR(−FeS) with K_3FeCN_6 (V_{max} = 66.3 ± 3.2 s^{-1}; K_m = 88.9 ± 10.7 μM) than in the comparable reaction in which PDR is the electron donor (V_{max} = 34.8 ± 0.3 s^{-1}; K_m = 6.0 ± 0.5 μM). Thus, although PDR(−FeS) is able to reduce ferricyanide at a maximum velocity that is about twice as great as that of PDR, it is a less efficient catalyst in this reaction. Clearly the FMN moiety of PDR(−FeS) is able to donate electrons to ferricyanide without the aid of the [2Fe−2S] domain of PDR. The rate of this reaction is slightly less than the rate of hydride transfer from NADH to the FMN (76 s^{-1}; see below), which is the limiting rate in the reductive half-reaction of PDR(−FeS). The maximal velocity of the electron transfer from PDR to ferricyanide closely matches the rate of the rate-limiting intramolecular electron transfer from the FMN to the [2Fe−2S] center of PDR (35 s^{-1}). These data are consistent with the idea that electron transfer from PDR(−FeS) to ferricyanide occurs directly through the FMN moiety and from PDR to ferricyanide through the [2Fe−2S] center.

Cofactor-Depleted Forms of PDR. We have generated forms of PDR [PDR(apoFMN), PDR(apoFeS), and PDR(apoFNN,apoFeS)] in which either or both the FMN and [2Fe−2S] centers have been depleted. We were able to reassemble the iron-sulfur center in the latter two apoproteins, resulting in PDR(+FeS) and PDR(apoFMN,+FeS). However, it was not possible to reconstitute PDR(apoFMN) or PDR(apoFMN,apoFeS) with FMN. Moreover, FMN is lost during the preparation of PDR(+FeS), such that the final product contains less than stoichiometric FMN. This is apparent in the spectrum of PDR(+FeS) in Figure 1B, which is approximately 50% depleted in FMN. Spectra of PDR(apoFMN,+FeS) and of PDR(−FMN) (Figure 1C) closely resemble the spectrum of adrenodoxin, suggesting that the [2Fe−2S] centers of these forms of PDR are intact.

Oxidation−Reduction Potentials of PDR(−FeS). The first and second electron potentials of PDR(−FeS) are separated by about 65 mV at pH 7 and 30 °C. Thus, under equilibrium conditions, two distinct reduction steps are observed. The first step involves the formation of a neutral blue flavin semiquinone (upper three spectra between 380 and 500 nm in Figure 3A). Subsequently, the enzyme is fully reduced to the flavin hydroquinone state (lower three spectra between 380 and 500 nm in Figure 3A). During the reduction process, the maximum concentration of semiquinone reached is about 60% of the total enzyme concentration (Figure 3B). The extinction coefficient of semiquinone at 527 nm was estimated by extrapolation of data in a plot of A_{527} vs A_{462} (data not shown). Species concentrations present during the reduction reaction were calculated using

$$C_{Flsq} = \frac{(A_T - C_T\epsilon)}{(\epsilon_{Flsq} - \epsilon)} \quad (1)$$

$$C_{Flred} = \frac{[A_r + (\epsilon_{Flox} - \epsilon_{Flsq})C_{Flsq} - \epsilon_{Flox}C_T]}{(\epsilon_{Flhq} - \epsilon_{Flox})} \quad (2)$$

$$C_{Flox} = C_T - (C_{Flsq} + C_{Flhq}) \quad (3)$$

where A_T is the total absorbance at 527 nm, C_T, C_{Flox}, C_{Flsq}, and C_{Flhq} are the concentrations of total, oxidized, semiquinone, and reduced forms of PDR(−FeS), and ϵ_{Flox}, ϵ_{Flsq}, and ϵ_{Flhq} are extinction coefficients of the oxidized, semiquinone, and reduced enzyme. ϵ is the extinction coefficient of oxidized and reduced enzyme at 527 nm, where the spectra of Fl_{ox} and Fl_{red} are isosbestic. C_{Flsq} was calculated using data collected at 527 nm, where ϵ = 1470 M^{-1} cm^{-1} and ϵ_{Flsq} = 5157 M^{-1} cm^{-1}. The extinction coefficient of pure semiquinone (ϵ_{Flsq}) was obtained by extrapolation of the data in a plot of semiquinone absorbance as a function of the extent of enzyme reduction at 527 nm. C_{Flhq} was calculated using data collected at 462 nm where ϵ_{Flox} = 13 400 M^{-1} cm^{-1}, ϵ_{Flsq} = 4482 M^{-1} cm^{-1}, and ϵ_{Flhq} = 2640 M^{-1} cm^{-1}. On the basis of these data, the semiquinone stability constant (K_{sq}) was found to be 8.1 ± 0.2.

$$K_{sq} = \frac{[Fl_{sq}]^2}{[Fl_{red}][Fl_{ox}]} \quad (4)$$

Estimates of the Fl_{ox}/Fl_{sq} and Fl_{sq}/Fl_{hq} potentials at pH 7 and 25 °C were based on the comparisons of enzyme redox transitions to those of indicator dyes of known potential. Species concentrations were calculated as a function of the extent of xanthine oxidase-mediated reduction reactions (Massey, 1991) using extinction coefficients determined for the oxidized and reduced forms of the indicator dyes and the oxidized and reduced forms of PDR(−FeS). Data condensed in log plots were fitted with

$$\log\left\{\frac{[PDR(-FeS)_{red}]}{[PDR(-FeS)_{ox}]}\right\} = n_1F\left(\frac{(E_{m7}(PDR(-FeS)) - E_{m7}(dye))}{2.303RT}\right) + \left(\frac{n_1}{n_2}\right)\log\left\{\frac{[dye]_{red}}{[dye]_{ox}}\right\} \quad (5)$$

Since the anthraquinone dyes used in these studies are found at equilibrium to exist in either the oxidized or two-electron-reduced state, with no detectable stabilization of semiquinone, n_2 (the number of electrons transferred per reduction of dye molecule) was fixed at 2.0. The number of electrons transferred per reduction of PDR(FeS) molecule, n_1, and the enzyme midpoint potential were optimized by the Marquardt−Levenberg fitting routine of the Kaleidagraph graphing and fitting program. The Fl_{ox}/Fl_{sq} potential of PDR(−FeS) (measured with anthraquinone-1,5-disulfonate) was found to be −170 ± 10 mV with n_1 = 0.99. The Fl_{sq}/Fl_{red} potential measured with anthraquinone-2-sulfonate was −235 ± 10 mV with n_1 = 1.3. These potentials are internally consistent. When the measured Fl_{sq}/Fl_{hq} potential was used as the reference point in eq 5, a value of −175 ± 10 mV

Scheme 1: Reaction of PDR(−FeS) with Pyridine Nucleotide[a]

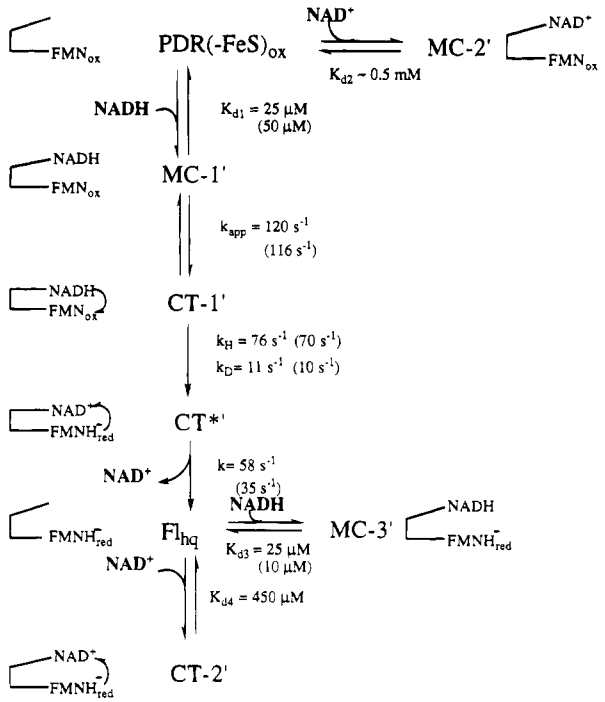

[a] Rate and equilibrium constants were determined by fitting procedures described in the text. Values in parentheses correspond to analogous steps in the reductive half-reaction of PDR.

was determined for Fl_{ox}/Fl_{sq} (n_1 = 0.94). Plots of enzyme reduction state as a function of solution potential are presented in Figure 3D.

Reaction of PDR(−FeS) with Pyridine Nucleotides. The reactions of PDR(−FeS) with NAD and NADH have been investigated by stopped-flow kinetic and equilibrium titrimetric methods. The mechanism of the reductive half-reaction of PDR(−FeS) based on these studies is presented in Scheme 1. Figure 4 contrasts data collected during the anaerobic reactions of similar concentrations of PDR (upper traces in each plot) and PDR(−FeS) (lower traces in each plot) with NADH. At 462 nm (Figure 4A) the initial absorbance and the total change in absorbance for reduction of PDR is nearly twice as great as for PDR(−FeS). This is due to the contribution of the oxidized iron−sulfur center to the PDR absorbance spectrum. Similarly, at 740 nm (Figure 4C), the initial and final absorbancies in the upper kinetic trace (PDR) are slightly larger than those of PDR(−FeS) due to the long-wavelength component of the iron−sulfur center in the PDR spectrum. Despite the absorbance offset in the reaction trace of PDR at 740 nm, similar absorbance changes are observed in both PDR and PDR(−FeS). These changes are thought to be due to formation and decay of charge-transfer complexes between flavin and pyridine nucleotide. The most striking difference in the reactions of these related enzymes is apparent in the data collected at 610 nm (Figure 4B). Following the hydride transfer event in PDR, NAD is released and an electron is transferred from the flavin hydroquinone to the oxidized [2Fe−2S] center. As NAD is released there is a decrease in absorbance due to the dissociation of the flavin hydroquinone-to-NAD charge-transfer complex; this is accompanied by a larger increase in absorbance due to the formation of the reduced iron-sulfur flavin semiquinone form of the

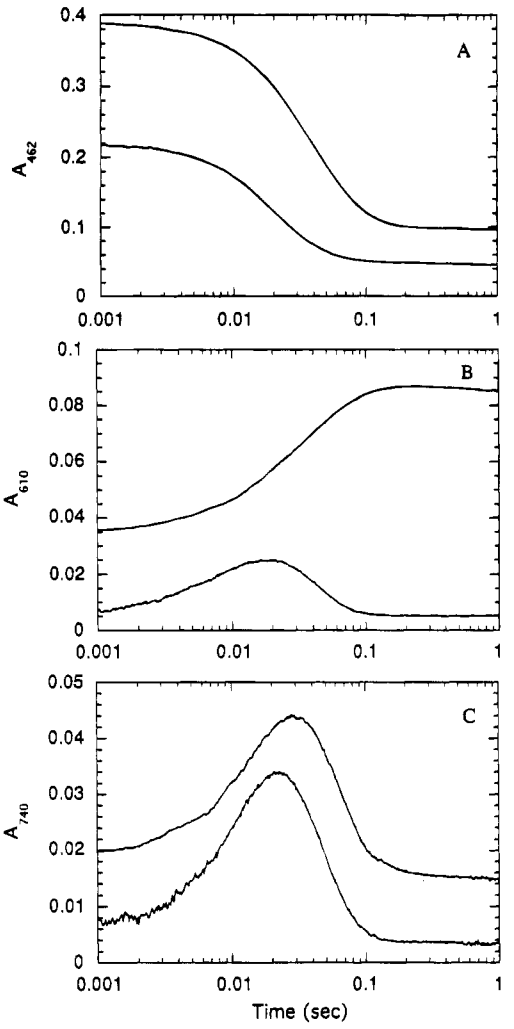

FIGURE 4: Comparison of the reaction of 16.1 μM PDR and 16.4 μM PDR(−FeS) with 100.8 μM NADH measured at 462, 610, and 740 nm. Upper traces in each plot are from reactions with PDR. Lower traces are from reactions with PDR(−FeS). (Data represent the average of 2−5 experimental determinations).

enzyme. The summation of these opposing absorbance changes results in a net increase in absorbance at 610 nm. The initial events and associated absorbance changes of NADH binding, hydride transfer, and NAD release in PDR(−FeS) parallel those observed in PDR; however, PDR(−FeS) is not able to undergo the intramolecular electron transfer event observed in PDR. Hence, no absorbance due to semiquinone formation occurs in the PDR(−FeS) reaction. The observed decrease in absorbance (10 ms − 100 ms at 610 nm) thus represents the decomposition of the Fl_{hq}-to-NAD charge-transfer complex as NAD is released from the hydroquinone form of the enzyme (an event that is obscured by the absorbance increase on semiquinone formation in PDR).

Pyridine Nucleotide Complexes of PDR(−FeS). NADH binds tightly and with apparently equal affinity to both the oxidized and hydroquinone states of PDR(−FeS). NAD also binds to these forms of the enzyme but with much lower affinity. This binding can be monitored by a strong long-wavelength charge-transfer band (Figure 5A). To quantify this interaction, PDR(−FeS) was photoreduced to the hydroquinone state and then titrated with NAD. A hyperbolic fit through the data at 740 nm gives a K_d of 450 ± 35 μM and an extinction for the complex (CT-2′ in Scheme 1) of 3100

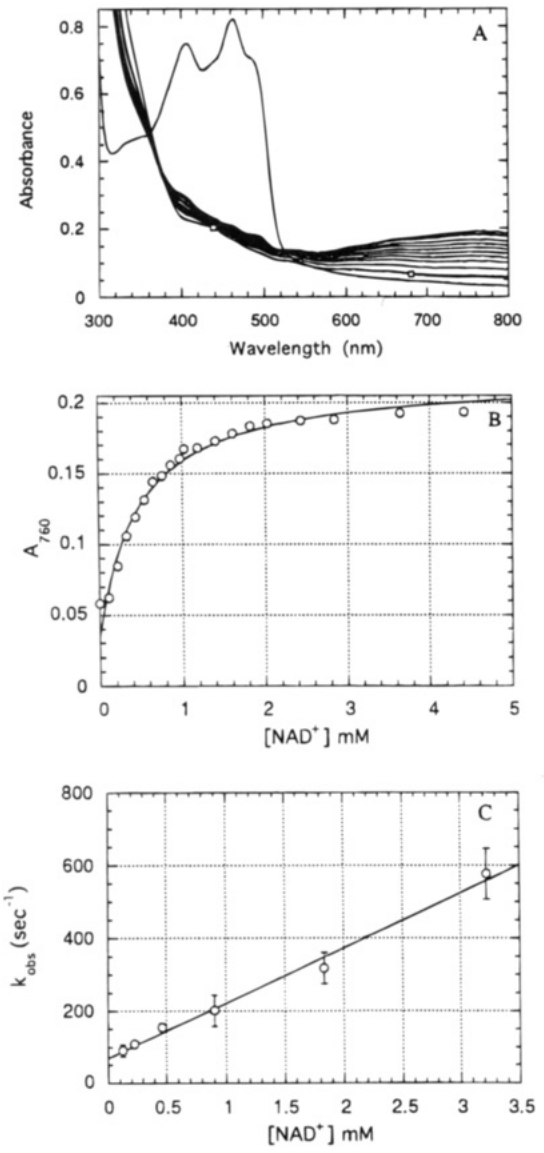

FIGURE 5: Formation of CT-2′, a complex of NAD and EFl_{red}. (A) Upper trace (at 460 nm) represents oxidized 61 μM PDR(−FeS) in 100 mM HEPES containing 5 mM EDTA, 100 μM PCA, 1 μM PCD, and 1 μM 5-deazaflavin (pH 8, 4 °C). Lowest trace at 460 nm represents PDR(−FeS) spectrum after ~3 min of photoreduction (effected by a 650-W Sun Gun). Anaerobic titration with NAD resulted in the increasing absorbance between 500 and 800 nm. (B) Data at 760 nm from panel A plotted as a function of NAD concentration and a hyperbolic fit through the data points. (C) Plot of observed rate constants of the reaction of photoreduced 13.8 μM PDR(−FeS) with increasing concentrations of NAD. Each data point is based on the fit to 3−6 averaged shots. Error bars indicate standard deviation. Curves represent least-squares fits to the data.

M^{-1} cm^{-1} at 760 nm (Figure 5B). K_d for CT-2′ to NAD was determined to be 460 μM in a complementary study of the kinetics of formation of this complex (Figure 5C). The best linear fit to the data gives $k_{on} = 1.5 \times 10^5$ M^{-1} s^{-1} and $k_{off} = 69$ s^{-1}. At high NAD concentrations, two additional slow phases were observed following binding. The amplitudes associated with these changes were very small and no attempt was made to extract information from these data.

NADH and NAD bind competitively with each other to the hydroquinone form of PDR(−FeS). Mixtures of NAD and NADH were mixed anaerobically with PDR(−FeS) (data at 610 nm depicted in Figure 6A). The K_d for the complex of the hydroquinone form of PDR(−FeS) and NADH (MC-3′ in Scheme 1) was found by fitting the data collected at 1

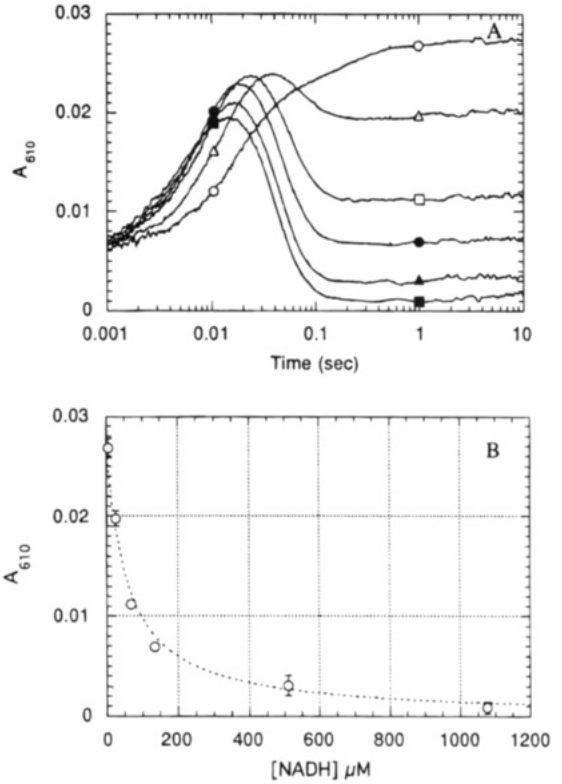

FIGURE 6: Reaction of 16.2 μM PDR(−FeS) with 0.6 mM NAD and various concentrations of NADH. (A) Absorbance changes observed at 610 nm. (○) 21.5 μM NADH, (△) 42.3 μM NADH, (□) 84.2 μM NADH; (●) 150.3 μM NADH, (▲) 527 μM NADH, and (■) 1.09 mM NADH. (B) (- - -) Fit to the data collected at (○) 610 nm at 1 s after mixing in the stopped-flow apparatus (see text).

s after mixing to the equation describing competitive binding:

$$A_T = \left\{\frac{(\epsilon_{Flhq}K_{d3}K_{d4} + \epsilon_{MC3'}K_{d4}[NADH] + \epsilon_{CT2'}K_{d3}[NAD])}{(K_{d3}K_{d4} + K_{d4}[NADH] + K_{d3}[NAD])}\right\}P_T \quad (6)$$

A_T is the total absorbance at 610 nm at 1 s after mixing. The values K_{d3} and K_{d4} represent the dissociation constants for the complexes MC-3′ and CT-2′, respectively. The extinction value ϵ_{Flhq} was set at 865 M^{-1} cm^{-1}, based on the spectrum of photoreduced enzyme. K_{d4} was fixed at 450 μM and $\epsilon_{CT2'}$ was fixed at 3100 M^{-1} cm^{-1}, based on the values obtained from the titration described above. The best fit to the data gives values of $\epsilon_{MC\text{-}3'} \sim 0$ and $K_{d3} = 24.1 \pm 4.5$ μM (Figure 6B). NAD and NADH also bind competitively to the oxidized form of PDR(−FeS). This is seen as a lag in the kinetics of enzyme reduction (Figure 6A, lowest two NADH concentrations). Simulations of this concentration dependence in accordance with the mechanism outlined in Scheme 1 suggest that the K_d values are approximately the same for the individual pyridine nucleotides binding to either oxidized or reduced forms of the enzyme ($K_{d1} \sim K_{d3}$ and $K_{d2} \sim K_{d4}$). However, NADH binds about 20-fold more tightly than NAD.

If NAD were to bind tighter to either oxidized or reduced PDR(−FeS), the midpoint potential would be shifted when NAD is added to the protein. Direct measurement of the influence of pyridine nucleotide binding on the flavin midpoint potential complements the results of the binding

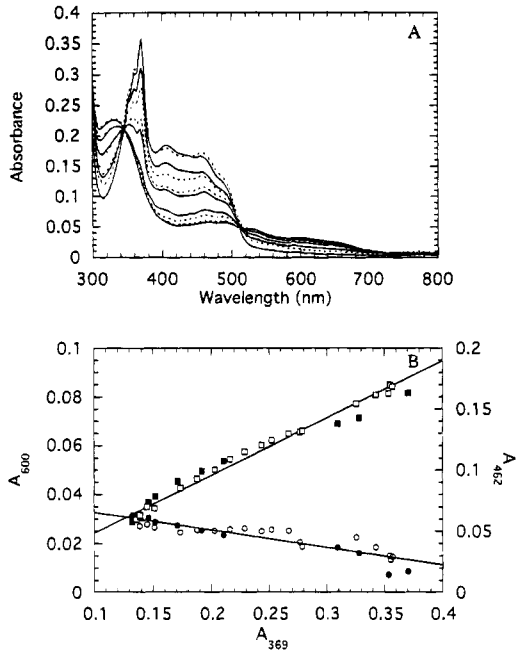

FIGURE 7: (A) (—) Spectra recorded during the photoreduction of 9.7 μM PDR(−FeS) in a mixture of 40 μM 1-OH-phenazine, 5 mM EDTA, and 200 nM 5-deazaflavin in 20 mM pH 7 phosphate buffer. (- - -) Spectra recorded during the oxidative titration of reduced PDR(−FeS) and 1-OH-phenazine with ferricyanide in the presence of 14 mM NAD. (B) Correlation of the extent of dye reduction measured at 369 nm and enzyme reduction measured at 600 nm (O, ●) and 462 nm (□, ■). The photoreduction is represented by solid symbols and ferricyanide reoxidation by open symbols.

studies. A mixture of 1-OH-phenazine (E_{m7} = −172 mV) and PDR(−FeS) (E_{m7} = −170 mV) were photoreduced anaerobically and then titrated with NAD (to about 30 times K_d). The sample was then oxidized by titration with potassium ferricyanide. Spectra representative of equilibrium states stabilized during the photoreduction and subsequent oxidative titration are presented in Figure 7A. A replot of the data from this reaction at 600 and 462 nm (representative of the enzyme redox state) as a function of the absorbance measured at 369 nm (representative of the indicator redox state) shows that, at corresponding points during the reductive titration (no NAD present) and the oxidative titration (saturating NAD), approximately equal fractions of oxidized and reduced dye and enzyme are present (Figure 7B). Thus, the flavin midpoint potential is not significantly influenced by bound NAD.

Reaction of PDR(−FeS) with NADH and NADD. The concentration dependence of the reaction of PDR(−FeS) with NADH is presented in Figure 8 at 462, 610, and 740 nm. Reaction traces simulated in accordance with the mechanism presented in Scheme 1 are superimposed on the data. The apparent first-order rate constants for the transitions from MC-1′ to CT-1′, CT-1′ to CT*′, and CT*′ to Fl_{hq} were estimated from exponential fits to the data as described in Gassner *et al.* (1994). The measured rates for these transitions were 120 s^{-1}, 76 s^{-1}, and 58 s^{-1}, respectively. Dissociation constants for the complexes MC-1′, MC-2′, MC-3′, and CT-2′ and the extinction coefficients for the complexes MC-3′ and CT-2′ were based on values obtained from the fits described above (Figures 5 and 6). The composition, redox state, and electronic spectrum of the species designated CT-2′ and CT*′ (Scheme 1) are very similar to each other,

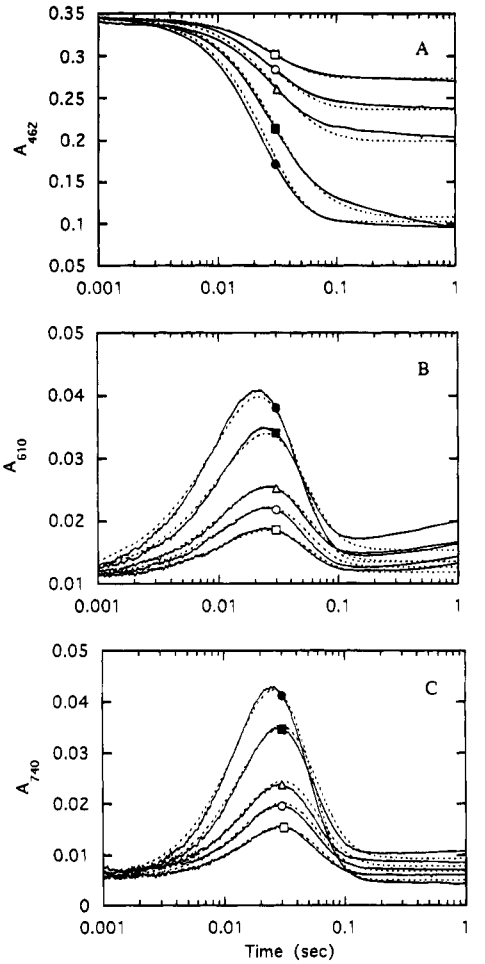

FIGURE 8: Concentration dependence of the reaction of 25.8 μM PDR(−FeS) with NADH observed at (A) 462, (B) 610, and (C) 740 nm. NADH concentrations: (□) 7.8 μM, (○) 11.8 μM, (△) 15.9 μM, (■) 31.4 μM, and (●) 62.1 μM. (- - -) Data simulation in accordance with the Scheme 1.

and it is possible that these represent the same structure. The analogous species CT* and CT-2 in the reductive half reaction of PDR (Gassner *et al.*, 1994) are clearly distinguished from each other in redox state (CT* contains an oxidized [2Fe−2S] center and a flavin hydroquinone; CT-2 contains a reduced [2Fe−2S] center and a flavin semiquinone). Kinetic data from the reductive half-reaction of PDR(−FeS) with NADH in the presence of NAD (see Figure 6) can be simulated in accordance with Scheme 1. Alternatively, the species CT-2′ can be eliminated from the simulation and the NAD release step (transition from CT*′ to Fl_{hq}) can be made reversible, such that in the presence of saturating NAD, the CT*′ complex rather than the CT-2′ complex is stabilized. The results of the data simulations which include or exclude CT-2′ fit the data equally well. It is likely that CT*′ and CT-2′ represent the same species; however, since there is a possibility that these NAD complexes have subtle structural differences, they are designated as separate species in Scheme 1. The extinction coefficients for MC-1′ and MC-2′ were set to match the extinctions of oxidized enzyme, and the extinctions of Fl_{red} were set to those of the enzyme after photoreduction. The extinction coefficients of the intermediate species, CT-1′ and CT*′, were varied until the best simulation of the data was obtained for the concentration dependence at each wavelength. Simulations treat the pyridine nucleotide binding

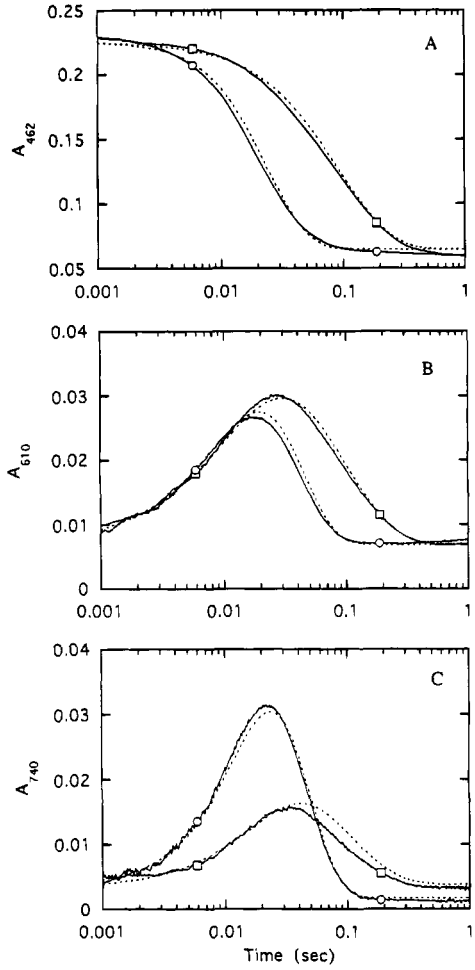

FIGURE 9: Reaction of 18.3 μM PDR(−FeS) with (○) 101 μM NADH or (□) 101 μM NADD at (A) 462, (B) 610, and (C) 740 nm. (- - -) Simulations in accordance with the mechanism outlined in Scheme 1.

steps as rapid equilibria followed by first-order steps in the reaction. At reaction times greater than 100 ms the simulations fit the data poorly at 610 nm (Figure 8B). The increase in absorbance at this wavelength is due to partial reoxidation of the enzyme to semiquinone. This is probably due to the reaction of the enzyme with a small amount of contaminating oxidant (oxygen, or ferredoxin domain). No attempt was made to simulate this portion of the reaction, since it is not reproducible.

In order to simulate the reaction of PDR(−FeS) with NADD (Figure 9), it was necessary to decrease k_2 (the apparent rate constant for hydride transfer) by a factor of 7. Substitution of NADD for NADH has the effect of decreasing the maximum observed concentration of the CT*′ intermediate formed during the reaction and increasing the maximum observed concentration of the CT-1′ intermediate, as predicted from Scheme 1. Simulations of species concentrations as a function of the extent of reaction indicate that, in the reaction of NADH with PDR(−FeS), the maximum concentration of the CT*′ intermediate occurs between 20 and 40 ms after mixing. In the reaction with NADD, the CT-1′ intermediate is the predominant species during this time period. As a result of their relatively large extinction coefficients, these charge-transfer complexes dominate the absorbance spectrum between 520 and 800 nm. The deuterium isotope effect thus enables partial kinetic and spectral resolution of these intermediates. Diode array

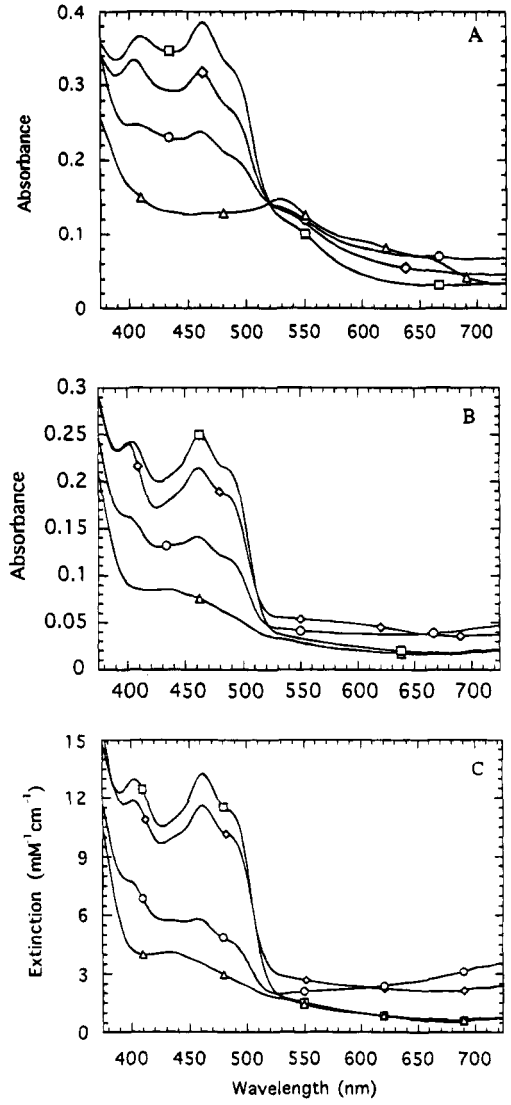

FIGURE 10: Diode array spectra recorded with the stopped-flow spectrophotometer during the reaction of PDR or PDR(−FeS) with reduced pyridine nucleotide (each spectrum represents a 2-ms exposure). (A) Reaction of 18.2 μM PDR with 101 μM NADH at average times of (□) 1, (○) 31, and (△) 71 ms after mixing and with (◇) 101 μM NADD at 31 ms after mixing. (B) Reaction of 20 μM PDR(−FeS) with 101 μM NADH at average times of (□) 1, (○) 21, and (△) 71 ms after mixing and with (◇) 101 μM NADD at 21 ms after mixing. (C) Spectra of intermediates derived by global analysis of the reaction of PDR(−FeS) with pyridine nucleotides: (□) PDR(−FeS)ox, (◇) CT-1′, (○) CT*′, and (△) Fl_{hq} and MC-3′.

spectra recorded 32 ms into the reaction of PDR(−FeS) with NADH, or NADD (Figure 10B), provide approximate spectral representations of the CT*′ and CT-1′ intermediates, respectively. Similarly, diode array spectra were recorded during the reaction of PDR with NADH, and NADD (Figure 10A), as a means of kinetically resolving the CT-1 and CT* intermediates in the holoenzyme [also see Gassner *et al.* (1994)]. Pure spectra of the intermediates CT-1′, CT*′, and MC-3′ were calculated from simulations of kinetic data acquired at single wavelengths in accordance with the mechanism presented in Scheme 1. These simulated intermediate spectra [calculated using the program HopKINSIM for the Macintosh (1990 version)] were in good agreement with spectra derived through global Marquardt fitting of diode array data using the program Specfit (Spectrum Software Associates, 1993) (Figure 10C). The diode array

data were acquired under pseudo-first-order reaction conditions, such that a sequential four-step model could be used in the global fitting. Since an excess of NADH is present, the fully reduced enzyme spectrum represents a mixture of Fl_{red}' and MC-3'.

DISCUSSION

The phthalate dioxygenase system provides a novel model for the study of electron transfer reactions and the control of these processes in biological systems. The dioxygenase and reductase components of the PDS are readily dissociated, allowing these proteins and their associated cofactors to be studied as subsystems; the modular structure of the reductase allows this protein to be further disassembled into FNR-like and ferredoxin-like components. Details of the mechanism of electron transfer in the PDS may be of broad significance since the cofactors employed in this system are common elements of photosynthetic, respiratory, and other electron transport chains.

We have generated iron−sulfur- and flavin-depleted forms of PDR using techniques similar to those employed in the study of benzoate dioxygenase (Yamaguchi & Fujisawa, 1981). These preliminary studies indicate that it is possible to generate both PDR(apoFeS) and PDR(apoFeS,apoFMN) and to reconstitute these proteins with iron−sulfur centers that are redox-active and stable at values of pH > 7. However, we have been unable to prepare or reconstitute these samples with stoichiometric FMN.

We have used chymotrypsin to remove the iron−sulfur domain of PDR and generate a truncated enzyme, PDR(−FeS), that is incapable of intramolecular electron transfer. The selectivity of this cleavage was initially quite surprising given the relatively broad specificity of chymotrypsin and the large number of potential cleavage sites in the PDR sequence. This result suggests that spatial localization of these sites in the PDR molecule makes them largely inaccessible to the active site of chymotrypsin. The peptide linker that is the site of proteolytic cleavage is one of two highly disordered regions in the crystal structure (Correll *et al.*, 1992). The solvent accessibility and disorder associated with this region make it particularly susceptible to chymotryptic cleavage. We were unable to recover the iron−sulfur domain, which is apparently proteolyzed following release from the PDR molecule. A good chymotrypsin cleavage site exists at L_{296}, which precedes the second, disordered, solvent-accessible loop region in the [2Fe−2S] domain (R_{297}−G_{302}). This cleavage could result in the loss of the iron−sulfur center ligand, C308, and disrupt the integrity of the [2Fe−2S] domain.

The FMN moiety remains tightly bound to PDR following the removal of the iron−sulfur domain. Inspection of the crystal structure of PDR predicts that all but one of the hydrogen-bonding amino acid side chains involved in binding and orienting the FMN are derived from the flavin binding domain. Only serine 274, which forms a hydrogen bond with the FMN ribityl side chain, is lost. Many amino acid side chains that surround the flavin dimethylbenzene ring in PDR (Arg 54, Arg 55, Thr 56, Ile 223, and Ser 224) are retained in PDR(−FeS). The most significant change is the loss of the amino acid loop (Ser 271−Cys 280) that contains the [2Fe−2S] center. The loss of this loop increases the solvent accessibility of the flavin and removes the influence of the iron−sulfur center, which has a net negative charge in its reduced form.

The relative effects of charge and polarity of amino acid side chains on the midpoint potential of FMN bound to flavodoxin have been investigated (Swenson & Krey, 1994). The primary effects of replacing Tyr 98 (one of two bulky aromatic residues that are close to the flavin) with arginine, which introduces a positive charge, is to decrease (−25 mV) the Fl_{ox}/Fl_{sq} potential and increase (+178 mV) the Fl_{sq}/Fl_{hq} potential. Similarly, it has been shown that replacement of negatively charged amino acids in the region of the flavin binding site of flavodoxin with neutral amino acids has virtually no effect on Fl_{ox}/Fl_{sq} but increases the Fl_{sq}/Fl_{hq} potential by about 15 mV for each neutralization of charge (Zhou & Swenson, 1995). PDR and PDR(−FeS) are similar to flavodoxin in that they both form neutral blue semiquinone on one-electron reduction and flavin hydroquinone anion on complete reduction. The Fl_{ox}/Fl_{sq} potentials of PDR and PDR(−FeS) are the same. Thus, as expected, the negative charge associated with the reduction of the [2Fe−2S] center of PDR has little effect on the oxidized/neutral semiquinone couple. However, the PDR_{2e-}/PDR_{3e-} potential is 50 mV more negative than the PDR(−FeS) Fl_{sq}/Fl_{hq} potential. It is possible the negative charge associated with the reduced iron−sulfur center depresses the flavin potential (PDR_{2e-}/PDR_{3e-} couple) in native PDR. On this premise we propose that the Fl_{sq}/Fl_{hq} couple of PDR(−FeS) is representative of the PDR_{1e-}/PDR_{2e-} couple in which both electrons are bound to the flavin. This intermediate state exists only transiently in the reductive half-reaction of PDR, just preceding intramolecular electron transfer from FMN to the [2Fe−2S] center. Thus, PDR(−FeS) provides a system in which the properties of this intermediate state and factors controlling intramolecular electron transfer in PDR can be studied.

An additional possibility is that the increase in redox potential of the Fl_{sq}/Fl_{hq} couple of PDR(−FeS) relative to that of PDR reflects increased solvent exposure of bound FMN. In flavodoxin, the main effect of replacing Tyr 98 with alanine is to increase the solvent accessibility of the flavin (Swenson & Krey, 1994). This results in a slight decrease (−38 mV) in the Fl_{ox}/Fl_{sq} potential and a larger increase (+139 mV) in the Fl_{sq}/Fl_{hq} potential. Presumably, the greater capacity for hydrating the Fl_{hq} anion stabilizes this state (Swenson & Krey, 1994).

Relative electron transferase activities of PDR and PDR(−FeS) with $K_3Fe(CN)_6$, DCPIP, and cytochrome *c* highlight the role of the [2Fe−2S] domain. These studies indicate that while small molecules such as DCPIP and ferricyanide may accept electrons from either FMN or the [2Fe−2S] center, cytochrome *c* accepts electrons exclusively through the [2Fe−2S] center. Similarly, phthalate dioxygenase (PDO) is restricted to accepting electrons through the [2Fe−2S] center of PDR (Gassner, 1995).

The intermediate species observed in the reductive half-reaction of PDR(−FeS) are spectrally very similar to the corresponding intermediates observed in the reductive half-reaction of PDR with NADH. Moreover, the kinetic constants relating intermediates in these mechanisms are nearly the same. Since these constants are related to the activation energies of the transition states involved in these reactions, we propose that PDR(−FeS) represents an excellent model system for investigating features of the reductive half-reaction of PDR that are not directly accessible in studies

of the holoenzyme. The comparison of PDR with PDR(−FeS) is particularly good, since we are able to judge the effect of the domain deletion on each step of the mechanism. Apparently, the ferredoxin-like and FNR-like domains of PDR do not interact in any way that significantly influences steps in the reaction mechanism preceding intramolecular electron transfer.

The intrinsic rate of the intramolecular electron transfer in PDR is predicted to be rapid given the short distance separating the FMN and [2Fe−2S] center and the favorable energetics of this reaction. If we assume that the Fl_{sq}/Fl_{hq} couple of PDR(−FeS) (−235 mV; no influence of iron−sulfur center) is representative of the SQ/HQ (iron−sulfur center oxidized) couple of PDR, then there is 65 mV, or −1.5 kcal·mol^{-1} driving force for intramolecular electron transfer and the conversion of HQ to SQ. Application of electron transfer theory developed by Marcus and Sutin (1985) to estimate the rate constant for a 4.7-Å through-space jump with a −1.5 kcal·mol^{-1} driving force at 4 °C gives an electron transfer rate constant of $>10^{10}$ s^{-1}.

Clearly, the rate or intramolecular electron transfer in PDR is much less than this theoretical limit. This is not a particularly uncommon scenario. In some cases electron transfer is gated by a relatively slow protein conformational change (Hoffman & Ratner, 1987). For instance, intramolecular electron transfer in cytochrome oxidase is thought to be linked to a rate-limiting conformational change associated with its function as a proton pump (Gray & Malmström, 1989). In addition, exposure of the donor and acceptor sites to solvent can greatly attenuate the rate of electron transfer between sites. It has been proposed that the difference in solvent content of the ubiquinone and menaquinone binding sites of the photosynthetic reaction center may account for the difference in the rate of electron transfer from these sites to the bacteriochlorophyll special pair (Dutton & Mosser, 1994); the rate of electron transfer from the type 1 site to the trinuclear copper site of laccase may also be greatly diminished due to the exposure of the acceptor site to solvent (Farver & Pecht, 1991).

Relatively slow rates of electron transfer have been measured in two systems that are more closely related to PDR. Electron transfer from ferredoxin to associated ferredoxin−NADP reductase occurs through a solvent-accessible interprotein interface region similar to the interdomain interface of PDR (Correll *et al.*, 1993); this electron transfer occurs with a rate constant on the order of only 10^3 s^{-1} (Walker *et al.*, 1991). A similar value has been measured by pH jump studies for the intrinsic rate of intramolecular electron transfer from the FMN to the [4Fe−4S] center of trimethylamine dehydrogenase, in which the flavin and iron center are separated by only 4 Å (Rohlfs & Hille, 1991; Lim *et al.*, 1986). A much slower value of intramolecular electron transfer has been measured in the reductive half-reaction of trimethylamine dehydrogenase with trimethylamine that is correlated with product release (Rohlfs & Hille, 1991; Steenkamp *et al.*, 1978).

Similarly, in the reductive half-reaction of PDR, the release of product (NAD) and intramolecular electron transfer from FMN to the [2Fe−2S] center are observed as a single kinetic phase (35 s^{-1}). The dissociation of NAD from the CT*′ intermediate of PDR(−FeS) occurs with a similar rate constant (58 s^{-1}) in the absence of intramolecular electron transfer. We propose that intramolecular electron transfer in PDR may ultimately be controlled by the rate at which NAD dissociates from the CT* intermediate. NAD bound to PDR in the CT* complex may prevent electron transfer either by raising the redox potential of the Fl_{sq}/Fl_{hq} couple to a value that stabilizes the flavin hydroquinone anion in the presence of an oxidized [2Fe−2S] center or by stabilizing a conformation of PDR that blocks intramolecular electron transfer.

The effect of charge-transfer complex formation on cofactor midpoint potential has been investigated in adrenodoxin and in ferredoxin−NADP reductases. A stable flavin hydroquinone-to-NADP charge-transfer complex is formed when reduced adrenodoxin reductase is titrated with NADP. This complexation apparently increases the midpoint potential of the Fl_{ox}/Fl_{hq} couple by about 100 mV (Lambeth & Kamin, 1976). The oxidation state and spectral features of this complex closely relate it to the CT* intermediate observed in the reductive half-reaction of PDR. In ferredoxin−NADP reductase, the flavin oxidized/flavin hydroquinone potential is not significantly influenced by associated NADPH (Batie & Kamin, 1986). However, the midpoint potential of NADP(H) bound to ferredoxin−NADP reductase is about 40 mV more positive than the free NADP/NADPH couple. This complex is more closely related to CT-1 in the reductive half-reaction of PDR. It can be concluded that the charge-transfer complexes stabilized by adrenodoxin reductase and FNR differ fundamentally both in terms of the donor and acceptor species involved in the complex and in terms of the effect of complexation on cofactor redox potential. If bound NAD has a similar effect on the redox potential of FMN in CT*, the thermodynamic driving force for electron transfer to the [2Fe−2S] center would be compromised until NAD is released from the enzyme. However, in PDR(−FeS), pyridine nucleotides are found to bind with equal affinity to oxidized and reduced forms of the enzyme, and potentiometeric measurements indicate that the midpoint potential of the Fl_{ox}/Fl_{sq} couple is not perturbed in the presence of saturating NAD. It thus appears that the slow intramolecular electron transfer in PDR is not controlled through modulation of the FMN midpoint potential as a result of the binding of pyridine nucleotides. On this basis we propose that the dissociation of NAD from CT* serves to switch PDR into a conformation that poises the system for rapid intramolecular electron transfer (eq 7).

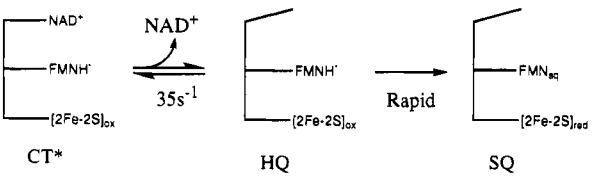

(7)

The EPR spectrum of PDR (SQ) (Batie *et al.*, 1991) shows very little magnetic interaction between the flavin radical and reduced [2Fe−2S] center in spite of the proximity of the two paramagnetic centers. EPR theory (Leigh *et al.*, 1970; Schepler *et al.*, 1975) has been applied in the analysis of the partially saturated EPR spectrum of SQ (Bertrand *et al.*, 1995). It has been possible to simulate this spectrum by invoking the "magic angle" of 131° between one of the **g**-tensors of the [2Fe−2S] center and the isotropic flavin radical. Verification of this special orientation awaits the determination of the **g**-tensor of the [2Fe−2S] center, which

is being carried out on single crystals of SQ and PDR_{3e-} (R. Dunham, D. Gatti, and R. H. Sands, personal communication). If the magic angle is indeed correct, then the two centers are not optimally oriented for magnetic interaction. According to Bertrand *et al.* (1995), this could significantly retard the intramolecular electron transfer event. We propose that an isomerization of protein structure triggered by the release of NAD from PDR may ultimately limit the rate of intramolecular electron transfer. Unfortunately, the intermediates CT* and HQ that precede the intramolecular electron transfer event are EPR-silent. Although we cannot definitively assign the structural influence of NAD binding to HQ at this time, it is likely to include the motion of phenylalanine 225 into a position that allows direct flavin−pyridine interaction.

Titration of fully reduced PDR(−FeS) with NAD results in the formation of the stable charge-transfer complex CT-2′, which is closely related to the CT* intermediate that occurs transiently in the reductive half-reaction of PDR. We hope to resolve this structure by X-ray crystallography.

ACKNOWLEDGMENT

We thank Drs. V. Massey, M. L. Ludwig, and W. R. Dunham for critical reviews of the manuscript and Dr. P. Andrews for helpful discussions pertaining to the mass and N-terminal sequence analysis. Support for these studies has been provided by National Institutes of Health Grant GM20877 to D.P.B.

REFERENCES

Ballou, D. P., & Batie, C. (1988) in *Oxidases and Related Redox Systems, 4th International Symposium*, (King, T. E., Mason, H. S., & Morrison, M., Eds.) pp 211−226, Walter deGruyter and Co., Hawthorne, NY.

Batie, C. J., & Kamin, H. (1986) *J. Biol. Chem., 261*, 11214−11223.

Batie, C. J., LaHaie, E., & Ballou, D. P. (1986) *J. Biol. Chem. 262*, 1510−1518.

Batie, C. J., Ballou, D. P., & Correll, C. C. (1992) *Chemistry and Biochemistry of Flavoenzymes* (Müller, F., Ed.) Vol. III, pp 543−556, CRC Press, Boca Raton, FL.

Bertrand, P., More, C., & Camensuli, P. (1995) *J. Am. Chem. Soc. 117*, 1807−1809.

Boxer, S. G. (1990) *Annu. Rev. Biophys. Biophys. Chem. 19*, 267−299.

Bull, C., & Ballou, D. P. (1981) *J. Biol. Chem. 256*, 12673−12680.

Burleigh, B. D., Foust, G. P., & Williams, C. H. (1969) *Anal. Biochem. 27*, 536−544.

Closs, G. L., & Miller, J. R. (1988) *Science 240*, 440−447.

Correll, C. C., Batie, C. J., Ballou, D. P., & Ludwig, M. L. (1992) *Science 258*, 1604−1610.

Correll, C. C., Ludwig, M. L., Bruns, C. M., & Karplus, P. A. (1993) *Protein Sci. 2*, 2112−2133.

Dutton, L. P., & Mosser, C. C. (1994) *Proc. Natl. Acad. Sci. U.S.A. 91*, 10247−10250.

Farver, O., & Pecht, I. (1991) *FASEB J. 5*, 2554−2559.

Gassner, G. T. (1995) Dissertation, University of Michigan, Ann Arbor, MI.

Gassner, G. T., Wang, L., Batie, C. J., & Ballou, D. P. (1994) *Biochemistry 33*, 12184−12193.

Ghisla, S., & Massey, V. (1986) *Biochem. J. 239*, 1−12.

Gray, H. B., & Malmström, B. G. (1989) *Biochemistry 28*, 7499−7505.

Hoffman, B. M., & Ratner, M. A. (1987) *J. Am. Chem. Soc. 109*, 6237−6243.

Hopper, D. J. (1976) *Biochem. Biophys. Res. Commun. 69*, 462−468.

Husain, M., & Massey, V. (1978) *Methods Enzymol. 53*, 429−437.

Jung, J., & Tollin, G. (1981) *Biochemistry 20*, 5124−5131.

Lambeth, J. D., & Kamin, H. (1976) *J. Biol. Chem. 251*, 4299−4306.

Leigh, J. S. (1970) *J. Chem. Phys. 52*, 2608−2612.

Lim, L. W., Shamala, N., Mathews, F. S., Steenkamp, D. J., Hamlin, R., & Xuong, N. H. (1986) *J. Biol. Chem. 261*, 15140−15146.

Lund, J., Woodland, M. P., & Dalton, H. (1985) *Eur. J. Biochem. 147*, 297−305.

Malkin, R., & Rabinowitz, J. C. (1966) *Biochem. Biophys. Res. Commun. 23*, 822−827.

Marcus, R. A., & Sutin, N. (1985) *Biochim. Biophys. Acta 811*, 265−322.

Massey, V. (1991) *in Flavins & Flavoproteins* (Curti, B., Ronchi, S., & Zanetti, G., Eds.) pp 60−66, Walter de Gruyter, Berlin.

Massey, V., & Hemmerich, P. (1977) *J. Biol. Chem. 252*, 5612−5614.

Massey, V., & Hemmerich, P. (1978) *Biochemistry 17*, 9−17.

Massey, V., & Hemmerich, P. (1980) *Biochem. Soc. Trans. 8*, 246−257.

Moser, C. C., Keske, J. M., Warncke, K., Farid, R. S., & Dutton, L. P. (1992) *Nature 355*, 796−802.

Neil, G. L., Niemann, C., & Hein, G. E. (1966) *Nature 210*, 903−907.

Rohlfs, R. J., & Hille, R. (1991) *J. Biol. Chem. 266*, 15244−15252.

Schepler, K. L., Dunham, W. R., Sands, R. H., Fee, J. A., & Abeles, R. H. (1975) *Biochim. Biophys. Acta 397*, 510−518.

Steenkamp, D. J., Singer, T. P., & Bienert, H. (1978) *Biochem. J. 169*, 361−369.

Swenson, R. P., & Krey, G. D. (1994) *Biochemistry 33*, 8505−8514.

Wikström, M., Krab, K., & Saraste, M. (1981) *Annu. Rev. Biochem. 50*, 623−655.

Yamaguchi, M., & Fujisawa, H. (1981) *J. Biol. Chem. 256*, 6783−6787.

Yamaguchi, M., & Fujisawa, H. (1982) *J. Biol. Chem. 257*, 12497−12502.

Yeh, W. K., Gibson, D. T., & Liu, T. N. (1977) *Biochem. Biophys. Res. Commun. 78*, 401.

Zhimin, Z., & Swenson, R. P. (1995) *Biochemistry 34*, 3183−3192.

BI950847L